Beam hardening correction for a cone-beam CT system and its effect on spatial resolution*

ZHAO Wei(赵维)[1,2,3;1)] FU Guo-Tao(付国涛)[1,2,3] SUN Cui-Li(孙翠丽)[1,2]
WANG Yan-Fang(王燕芳)[1,2] WEI Cun-Feng(魏存峰)[1,2] CAO Da-Quan(曹大泉)[1,2,3]
QUE Jie-Min(阙介民)[1,2] TANG Xiao(唐晓)[1,2,3] SHI Rong-Jian(史戎坚)[1,2]
WEI Long(魏龙)[1,2] YU Zhong-Qiang(郁忠强)[1,2]

[1] Key Laboratory of Nuclear Analytical Techniques, Institute of High Energy Physics, CAS, Beijing 100049, China
[2] Beijing Engineering Research Center of Radiographic Techniques and Equipment, Beijing 100049, China
[3] Graduate University of Chinese Academy of Sciences, Beijing 100049, China

Abstract: In this paper, we present a beam hardening correction (BHC) method in three-dimension space for a cone-beam computed tomography (CBCT) system in a mono-material case and investigate its effect on the spatial resolution. Due to the polychromatic character of the X-ray spectrum used, cupping and streak artifacts called beam hardening artifacts arise in the reconstructed CT images, causing reduced image quality. In addition, enhanced edges are introduced in the reconstructed CT images because of the beam hardening effect. The spatial resolution of the CBCT system is calculated from the edge response function (ERF) on different planes in space. Thus, in the CT images with beam hardening artifacts, enhanced ERFs will be extracted to calculate the modulation transfer function (MTF), obtaining a better spatial resolution that deviates from the real value. Reasonable spatial resolution can be obtained after reducing the artifacts. The 10% MTF value and the full width at half maximum (FWHM) of the point spread function with and without BHC are presented.

Key words: beam hardening correction, cone-beam computed tomography, spatial resolution

PACS: 81.70.Tx **DOI:** 10.1088/1674-1137/35/10/018

1 Introduction

Computed tomography (CT) is an imaging method used to produce two-dimensional or three-dimensional distribution (usually some physical properties such as density or attenuation coefficients) of objects from a series of X-ray projections when X-ray penetrates the rotating objects. The projection, which is a line integral of a single slice in the object, is a function of the X-ray energy, X-ray propagation length and the linear attenuation coefficients of the object. Since most materials absorb low-energy X-ray better than high-energy X-ray photons, mainly because of photoelectric absorption, the attenuation at a fixed point in an object is generally greater for photons of low energy [1]. Thus the energy distribution spectrum of the polychromatic X-ray beam changes (mean energy rise, namely beam hardening) as it passes through the object. A basic assumption for CT is that X-rays are attenuated in the same way in a particular voxel for every projection angle independent of how much matter the X-rays have penetrated before reaching the voxel [2]. This means monoenergetic X-rays are required. However, in practical CT imaging, a polyenergetic X-ray source (usually X-ray tubes) is employed, which means the amount of photons taken away from the beam is dependent on how deep the beam has propagated.

So when a voxel is located at the edge of the object facing the X-ray source, the mean energy of the X-ray spectrum reaching the voxel is lower and the number of photons attenuated from the beam as it

Received 24 January 2011, Revised 18 April 2011
* Supported by National Natural Science Foundation of China (10905063) and Instrument Developing Project of Chinese Academy of Sciences (2010024)
1) E-mail: zhaow@ihep.ac.cn

penetrates the voxel is larger. Meanwhile, when the object is turned to face the detector in later projections, the X-ray beam have to propagate a long path before reaching the voxel, which causes a higher mean energy since low energy photons are taken away from the beam. This gives a smaller density or attenuation coefficient of the material for the voxel in the latter projection than in the former. Thus, for the CT imaging with polyenergetic source the pixel values are dependent both on the voxel itself and where it is located, in contrast to the imaging with monoenergetic source which is only dependent on the material in the voxel. Beam hardening induces artifacts in CT imaging showing a smaller density in the center of the object namely cupping artifact and dark streaks between the region of high density [1, 3, 4]. The artifact can be explained by the nonlinear nature of beam hardening.

Beam hardening artifacts can be widely seen in CT images and bring difficulty to understand the object structure. They also severely limit the performance of quantitative analysis of the CT images [1]. There are many correction approaches proposed to reduce the artifacts. They can be classified into [5]: pre-filtering, linearization, dual energy and post-reconstruction method.

The spatial resolution characterizes the ability of a CT system to image fine structural detail. It is best quantified by a measurement of the point spread function (PSF) of the system or, equivalently, by the MTF, the frequency-space representation of the PSF. The recommended method is to determine the MTF by computing the amplitude of the Fourier transform of PSF. The PSF is obtained by calculating the derivative of the profile of the edge of a test phantom [6]. For a CBCT system, we choose a uniform steel ball as the test phantom. The diameter of the ball is 0.5 mm. In the reconstructed CT images, beam hardening artifacts enhance the edge of the ball. ERFs extracted from the enhanced edge cause a better modulation at higher frequencies, namely a better system spatial resolution.

Casteele [7] has investigated the effect of beam hardening on the resolution for fan beam reconstruction. In this paper, we investigate the effect of beam hardening artifacts on spatial resolution for cone beam reconstruction. In Part 2, we present the BHC method for the CBCT system which is based on the reprojection and linearization in a mono-material case. Beam hardening artifacts in the CBCT system can be corrected by the projection data and is independent of the reconstruction algorithm, so the BHC method for fan beam can be employed to correct the beam hardening artifacts in the CBCT system. In Part 3, we give the measurement and calculation of the MTF, in addition, the PSF fitted by Gaussian function which can show the FWHM is also presented. In Part 4, we give the BHC results of the steel ball, the MTF of the CBCT system and the FWHM of PSF with and without BHC. We also give the deviation of the calculation. For a CBCT system, beam hardening artifacts lead to an asymmetry PSF, causing a better spatial resolution which deviates from the real value. After reducing the beam hardening artifacts, the PSF recovers symmetry. Reasonable spatial resolution can be calculated.

2 Method

2.1 BHC for the CBCT system

In a CBCT system, usually a flat-plane detector or a CCD array is employed. The X-rays diverge from the X-ray source and form a cone-like solid angle, shown in Fig. 1. A divergent line which connects the X-ray source spot and the detector pixel represents the X-rays penetrating the object. The whole object can be reconstructed from one single scan. Compared with BHC for the fan beam CT, BHC for the CBCT system need to solve two problems:

1) The mid-plane and off mid-plane can use the same correction model.

2) BHC for the CBCT system is independent of reconstruction algorithm, just as BHC for the fan beam CT.

The explanations for the two questions go as follows:

1) When a polyenergetic X-ray beam passes through an object, the exit intensity can be expressed as

$$I = I_0 \int_0^{E_0} S(E) D(E) \mathrm{e}^{-\sum_{j=1}^{M} \mu_j(E) X_j} \mathrm{d}E \qquad (1)$$

and

$$\int_0^{E_0} S(E) D(E) \mathrm{d}E = 1, \qquad (2)$$

where I_0 is the incoming photon intensity and $S(E)$ is the polychromatic X-ray spectrum. $D(E)$ is the energy dependent efficiency of the detector and $\mu_j(E)$ is the linear attenuation coefficient of the jth material along the path, X_j is the length of the jth material and E_0 is the maximum photon energy in the spectrum.

Define ray sum R,

$$R(\mu, x) = -\ln\left(\frac{I}{I_0}\right). \qquad (3)$$

Then

$$R(\mu,x)=-\ln\int_0^{E_0}S(E)D(E)\mathrm{e}^{-\sum_{j=1}^{M}\mu_j(E)X_j}\mathrm{d}E. \quad (4)$$

So the ray sum R for a divergent line which connects the X-ray source spot and the detector pixel is a function of the linear attenuation coefficient μ of the material along the path and the propagation path length x. When there is a mono-material in case, R is dependent on propagation path length x and is independent on the location of the propagation voxel. Thus the correction model constructed by the projection data in off mid-plane is the same as the correction model constructed in mid-plane, which means we can use the mid-plane correction model to correct the off mid-plane projection data.

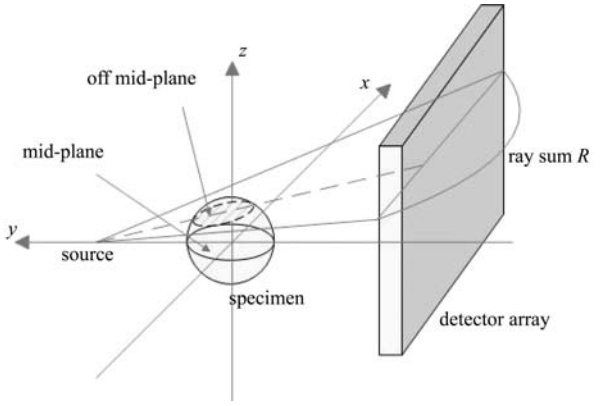

Fig. 1. The cone-beam reconstruction arrangement.

2) Let $R(L)$ be the measured CT raw ray sum (log attenuation) and let $R_{\mathrm{c}}(L)$ be the desired corrected raw ray sum that corresponds to the line of integration L (or detector channel number). We define

$$R_{\mathrm{c}}=\psi(R), \quad (5)$$

where ψ is the correction function, for convenience we drop the index L here, then the required amount of correction

$$\Delta R=R_{\mathrm{c}}-R. \quad (6)$$

Since CT reconstruction is a back-projection procedure, it can be formulated by inverse Radon transform. If $f(\vec{r})$ is a reconstructed image with reduced beam hardening artifact, for the fan beam CT, we have

$$f(\vec{r})=\Re_2^{-1}R_{\mathrm{c}}=\Re_2^{-1}(R+\Delta R)=\Re_2^{-1}R+\Re_2^{-1}\Delta R, \quad (7)$$

where $\Re_2^{-1}$ represents a 2D inverse Radon transform, in the last step, we use the linearity of the Radon transform. For the CBCT system, we also have

$$f(\vec{r})=\Re_3^{-1}R_c=\Re_3^{-1}(R+\Delta R)=\Re_3^{-1}R+\Re_3^{-1}\Delta R, \quad (8)$$

where $\Re_3^{-1}$ represents a 3D inverse Radon transform. From the above two equation, we know that BHC for fan beam CT and BHC for the CBCT are both independent of reconstruction algorithm as the linearity nature of the Radon transform. Thus the BHC model of the fan beam CT can be used to correct the projection data of the CBCT system.

The BHC method used in this paper is based on linearization and reprojection. The basic idea of linearization is to transform the ray sum values from the curved function $R_{\mathrm{poly}}(X)$ to values on the linear function $R_{\mathrm{mono}}(X)$, for the same objects thickness. Then we have

$$R_{\mathrm{poly}}(X)=\sum_{l=1}^{N}a_lX^{l-1}, \quad (9)$$

where a_l is the polynomial coefficient and X is the propagation path length. The slope of $R_{\mathrm{poly}}(X)$ at $X=0$ can be considered as the attenuation coefficient when monoenergetic X-ray is employed. Then the corrected ray sum value is $R_{\mathrm{mono}}=a_1X$.

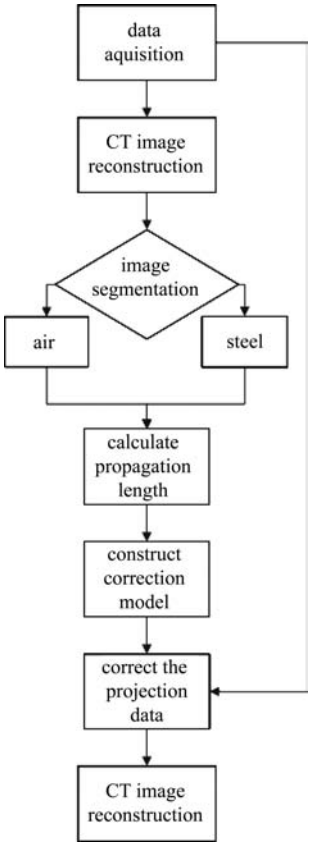

Fig. 2. The BHC flow chart for the CBCT system.

The drawback of linearization is that it requires calibration measurement of $R_{\mathrm{poly}}(X)$ for different thicknesses of the object material. This can be laborious and sometimes impossible in reality, such as BHC for CT image of ancient fossils. To avoid this fact, we introduce the reprojection procedure to construct the

correction model [5]. The correction method can be explained by the flow chart in Fig. 2.

First the raw projection data are reconstructed and then the CT image is segmented to distinguish the steel and the surrounding air by the OTSU segmentation algorithm [8]. After that, the propagation path length within object for each pixel is calculated by a ray tracing algorithm and the pixel size of CT image which is calculated by the magnification. The calculated length is then assigned to the corresponding measured ray sum R_{ij} to construct the correction model. The raw projection data are corrected by the correction model. Finally, the corrected raw data are reconstructed, resulting in CT images with reduced beam hardening artifact. Since the off mid-plane data and the mid-plane data can use the same correction model, in this paper, we only construct the mid-plane correction model which can save a lot of time. Compared with other BHC methods, we can see that the BHC method based on linearization and reprojection doesn't need calibration measurement, X-ray spectrum or material characteristics (such as mass attenuation coefficients or mass energy-absorption coefficients). The method only needs raw projection data and the correction procedures are very convenient.

2.2 Spatial resolution measurements

Spatial resolution for the CBCT system is measured with and without BHC according to the standard ASTM E1695-95 [6] and a preprint in our group [9]. Compared with the fan beam CT system, in the CBCT system, we use a steel ball (0.5 mm in diameter) as the test phantom. Put the ball in the field of view of the CBCT system and the position doesn't need to be in the center of rotation stage. 3D CT images with beam hardening artifact are reconstructed by the raw projection data, while 3D CT images without beam hardening artifact are reconstructed by the corrected projection data. The MTF measurement is based on the two sets of 3D CT images.

We measure the MTF and the FWHM of the PSF on XY, YZ and ZX planes that pass through the center of the ball (the rotation axis is Z axis) with and without BHC. The measured procedure goes as follows:

1) In the reconstructed 3D images, extract a sub volume containing the steel ball. The size of the volume should be larger than the diameter of the ball. For example, we extract a $239 \times 239 \times 239$ volume.

2) Find the center of the steel ball.

On XY plane, find the edge of the ball in different slices using the Canny edge detection algorithm [10]. Use a circle to fit the edge by employing the least-square method. Then we can get the diameter and the center of the circle X_{center}, Y_{center}. The center of steel ball locates on the slice Z_{center} which gives the largest circle diameter. So the center of the steel ball is X_{center}, Y_{center}, Z_{center}. On YZ, ZX planes, use the same method to find the center of the steel ball and the maximum diameter of the fitting circle. The deviation of the center of the steel ball and the maximum diameters of the fitting circle found on different planes which depend on the roundness of the steel ball should be smaller than 1 pixel. In this experiment, the relative roundness of the steel ball is 0.6% which can satisfy the requirement.

3) Obtain the ERF in the CT image.

In the sub volume, on XY plane, obtain 36 sets of line profiles that pass the center of the steel ball with a 10 degree increment. Use the same method to obtain 36 sets of line profiles on YZ and ZX planes, respectively. All of the profiles are then averaged. The averaged line profile includes two ERFs corresponding to two edges of the steel ball.

4) Calculate the differentiation of the averaged ERF to obtain the Line-Spread Function (LSF), which can be roughly equivalent to PSF.

5) Calculate the Discrete Fourier Transform of the PSF and normalize the magnitude at zero frequency to unity to generate the MTF. The 10% MTF value is often used to characterize the spatial resolution of the CT system.

6) In order to show the deviation of the calculated spatial resolution, redo Procedure 3) to 5) thirty times with different sampling angles. Then we can obtain 30 normalized MTF and 30 corresponding 10% MTF values. The deviation of the spatial resolution is from these 10% MTF values.

7) Fit the PSF to obtain the FWHM.

In order to obtain the FWHM of the PSF, we use the single parameter Gaussian function to fit the PSF. Since the FWHM is another parameter to characterize the performance of the system, we can compare the FWHM with the 10% MTF value. According to the relationship between the standard deviation σ of the Gaussian function and the FWHM,

$$\text{FWHM} = 2.3547\sigma, \tag{10}$$

we can easily calculate the FWHM by σ which is given by the least-squares fitting. The procedure to obtain the deviation of the FWHM is similar to Procedure 6). Obtain 30 averaged ERFs with different sampling angles. Calculate the differentiation and fit them with Gaussian function. We can obtain 30 FWHMs and

the standard deviation of the 30 FWHMs is the deviation of the result.

3 Apparatus and implementation

The experiment is performed on a 225 kV cone-beam micro-CT system. The system is developed and built by the Institute of High Energy Physics (IHEP), the Chinese Academy of Sciences (CAS). The main system components are an amorphous silicon Flat Panel Detector (FPD), an X-ray tube and a rotation stage. The FPD (PaxScan 4030CB, Varian Medical System, UT, America) compact 2048×1536 194 μm-pixel array and the conversion screen are integral columnar CsI(Tl). The X-ray tube (Phoenix xs-225d, GE, America) has a 5 μm–15 μm focal spot. The rotation stage (Huber 410A, Huber, Germany) has a resolution of 0.001°/1000 steps.

The experimental setting is shown in Table 1.

Table 1. The experimental setting.

voltage	120 kVp
current	40 μA
projection number	1800
magnification	60
reconstructed image size	2048×2048

Scan the steel ball at conditions given in Table 1. The projection data are first reconstructed by the FDK algorithm to generate CT images with beam hardening artifacts. Then the projection data are corrected by the BHC method presented in Section 2.1. Finally, the corrected projection data are reconstructed to generate CT images with reduced beam hardening artifacts. For convenience, in the reconstructed 3D image we extract a sub volume containing the steel ball in a $239\times239\times239$ array. The spatial resolution is calculated by the procedures presented in Section 2.2 which are based on the two sub volumes, with and without BHC.

4 Results

4.1 Beam hardening correction

In the following section, the reconstructed CT images with and without BHC are presented. Following the BHC procedures discussed before, firstly, the edge of the ball is detected by the Canny algorithm, seen in Fig. 3(b). Then the center and the diameter of the ball are found by performing a least-square circle fitting. The mid-plane of the CT image is segmented to distinguish the steel and the surrounding air, as shown in Fig. 3(a). After that, the propagation path length for each pixel in the mid-plane is computed and the results are assigned to the raw ray sum of the corresponding pixel to construct the correction model. In Fig. 4, the line and curve represent the monoenergetic and polyenergetic ray sums, respectively. The relationship between the computed propagation path length and the raw ray sum is non-linear due to the beam hardening effect. Fitting the curve with a fourth-degree polynomial, then the corrected ray sum can be calculated by the slope of the polynomial at original point. The corrected ray sum is filtered with a 2D median filter because the correction process can magnify noise. The results of CT images without

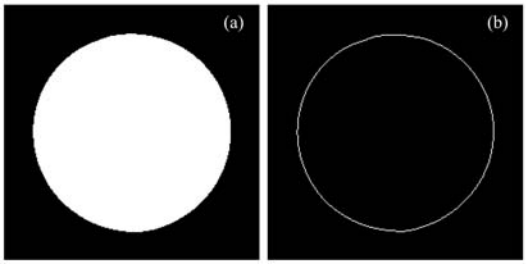

Fig. 3. (a) Binarizated CT image that passes the center of the steel ball. The white area is the ball and the dark area is the surrounding air. (b) The Detected edge of the ball by performing Canny algorithm.

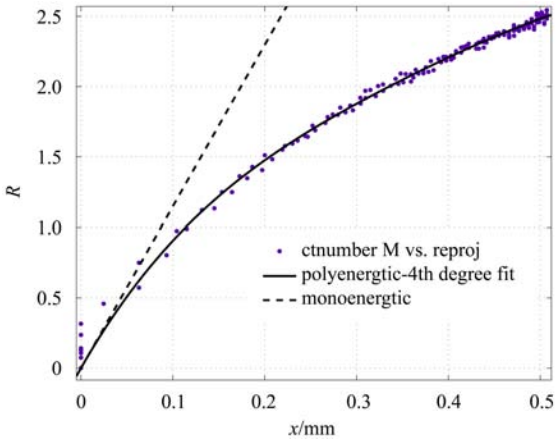

Fig. 4. The relationship between the propagation path length and the ray sum of the steel ball. The X-axis is the propagation path length and is labeled as millimeter. The Y-axis is the ray sum. The solid line is the polyenergetic ray sum fitted by a 4^{th} polynomial. The non-linearity nature of the curve characterizes attenuation when the polyenergetic X-ray passes though an object. The dotted line shows the linear attenuation nature when the monoenergetic X-ray passes through an object. Both of the lines pass though the original point.

BHC are shown in Figs. 5(a)–(c). The cupping artifacts can be clearly seen in the images of different planes and gray levels of the images aren't uniform. The line profiles of the uncorrected CT images in Figs. 5(g)–(i) show that the larger the distance to the center of the steel ball is, the higher the gray levels of the images have, as the reason of beam hardening. We can see that the descent of the gray level of the steel ball besides the edge causes an enhanced edge. CT images on different planes reconstructed by the corrected ray sum are shown in Figs. 5(d)–(f). We can see that the CT images are much uniform with reduced beam hardening artifacts. The line profiles of the corrected CT images shown in Figs. 5(g)–(i) reveal that the cupping artifacts are reduced almost completely.

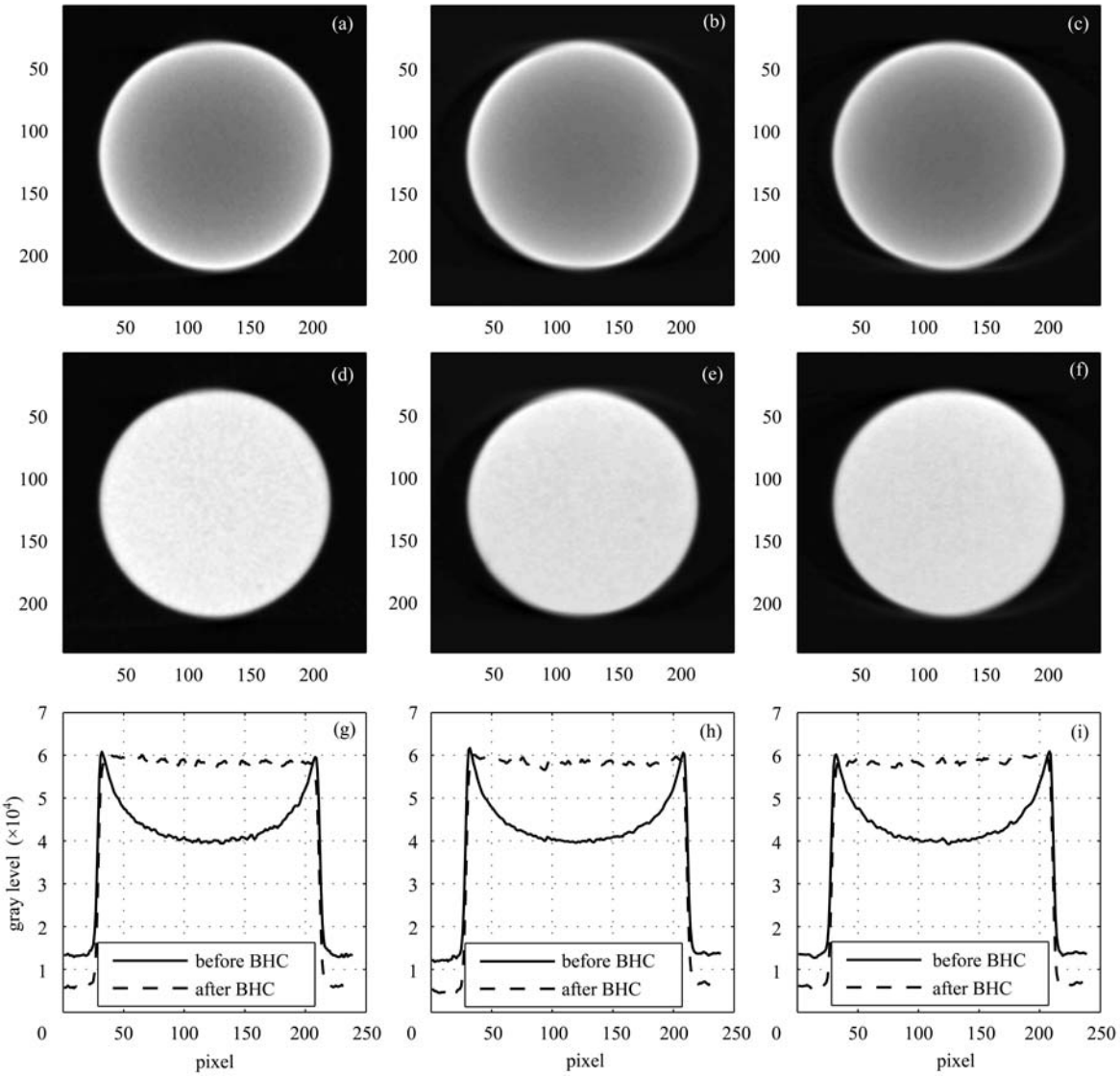

Fig. 5. CT images with and without BHC on different planes and the line profiles that pass the center of the ball. Column 1, 2, 3 represent the CT images and the line profiles on the XY, YZ and XZ planes, respectively. Row 1, 2, 3 represent the CT images without BHC, with BHC and line profiles, respectively.

4.2 Spatial resolution

In this section, the MTF and the FWHM of the PSF are presented. The averaged ERF is obtained according to the procedures discussed before. Then it is differentiated to yield the PSF, seen in Fig. 6. Due to the enhanced edge caused by the beam hardening effect, the PSF is no longer symmetrical. The side of the PSF that corresponds to the steel ball has much severer descent, meanwhile, the extension of the PSF that corresponds to the ball deviates from 0. After the BHC, the cupping artifacts and the en-

hanced edge are reduced and the PSF recovers symmetry that it shall be. The extension of the PSF that corresponds to the ball recovers 0. The FWHM of the PSF is obtained by performing a Gaussian fitting on the PSF with and without BHC, shown in Fig. 7. The FWHM of the PSF with BHC is larger than the PSF without BHC that means we get a better spatial resolution before BHC. According to the geometry relationship, we can calculate the physical size of the pixel in CT image (2.74 μm). Thus the FWHM of PSF can be represented in physical size. Calculating the Discrete Fourier Transform of the PSF and normalizing the magnitude at zero frequency to unity, we get the MTF, shown in Fig. 8. The 10% MTF value without BHC is larger than the 10% MTF value with BHC which is consistent with the results of the FWHM. The results of the FWHM and 10% MTF values with and without BHC are listed in Table 2.

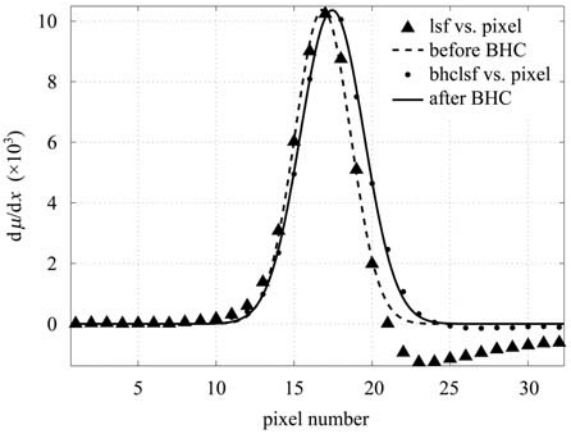

Fig. 7. The PSF with and without BHC fitted by the Gaussian function. Beam hardening artifacts lead to a narrower PSF, causing the FWHM to deviate from the real value. The X-axis is the pixel number and the Y-axis is $\mathrm{d}\mu/\mathrm{d}x$.

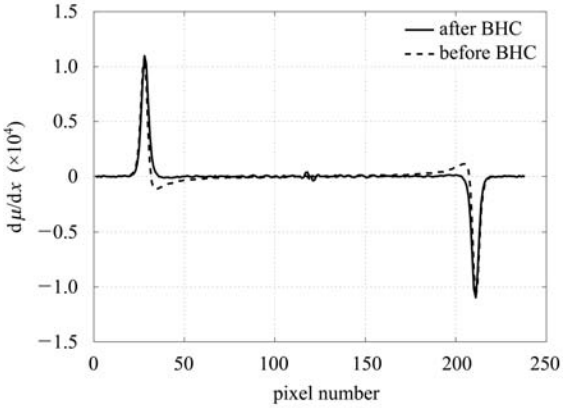

Fig. 6. The PSF with and without BHC. The PSF is no longer symmetrical due to the enhanced edge caused by the beam hardening effect. After BHC, the symmetry is recovered. The X-axis is the pixel number and the Y-axis is $\mathrm{d}\mu/\mathrm{d}x$.

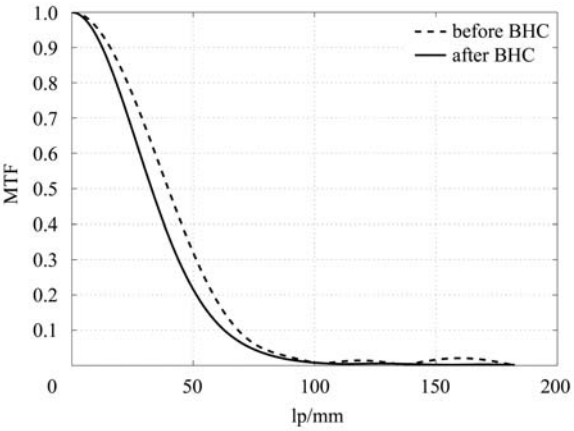

Fig. 8. The MTF with and without BHC. The 10% MTF value is much higher without BHC. The X-axis is the space frequency represented as lp/mm and the Y-axis is the normalized MTF.

Table 2. Spatial resolution of the CBCT system.

spatial resolution	10%MTF/(lp/mm)	FWHM(voxel)	FWHM/μm
without BHC	68.52±0.28	4.18±0.01	11.45±0.03
with BHC	63.15±0.33	4.79±0.02	13.12±0.05

Deviations of the results are calculated as discussed before. Deviations become larger after BHC because BHC can magnify the projection noise.

5 Discussion and conclusion

Since the CBCT system is a spatial variant system [11], the ball diameter shouldn't be too big. Meanwhile, the ball diameter should be big enough compared with the spatial resolution which can be satisfied in our experiment. So the ball chosen in our experiment is reasonable. Besides, the averaged ERF is very sensitive to the roundness of the ball, so it's very important to guarantee the roundness of the ball. The relative roundness of the ball is 0.6%, which satisfies the requirement.

An uniform steel ball is no longer uniform in the reconstructed 3D CT images due to the beam hard-

ening effect. The larger the distance to the ball center is, the higher the gray levels of the CT images have. Beam hardening artifacts on any plane are the same as the beam hardening artifacts in 2D space. The 3D CT images are uniform after BHC and the cupping artifacts on any plane are reduced.

In this paper, we perform BHC in a mono-material case for the CBCT system and prove that beam hardening artifacts cause an enhanced edge and induce an asymmetrical PSF. Thus the spatial resolution which is calculated by the ERF deviates from the real value. The PSF recovers symmetry and the spatial resolution is close to the real value when the artifacts are reduced. So the calculated spatial resolution is reasonable when the beam hardening artifacts are reduced or the beam hardening artifacts can be neglected.

We are grateful to the referee, whose comments led to the improvement of this paper. We also wish to express our thanks to the Imaging Engineering Group for useful discussion and to HUANG Huan, YANG Zhe-Ying and YANG Sheng-Yu for technical support.

References

1 Hsieh J. Computed Tomography: Principles, Design, Artifacts, and Recent Advances. SPIE Press, 2003. 221–230
2 Hammersberg P, Mangrad M. Journal of X-ray Science and Technology, 1998, **8**: 75–93
3 Kak A C, Slaney M. Principles of Computerized Tomographic Imaging. IEEE Press, 1988. 120–125
4 Kijewski P K, Bjarngard B E. Med. Phys., 1978, **5**: 209–214
5 Krumm M, Kasperl S, Franz M. NDT&E International, 2008, **41**: 242–251
6 E1695-95. Tech. Rep., American Society for Testing and Material (ASTM), 1995
7 Casteele E V, Dyck D V, Sijbers J et al. Proceedings of SPIE, 2004, **5370**: 2089
8 Otsu N. IEEE Transactions on SMC, 1979, **9**(1): 62–66
9 WANG Y F et al. This work is preparing
10 Canny J. IEEE Transactions on Pattern Analysis and Machine Intelligence, 1986, **PAMI-8**(6): 679–698
11 CHEN Zi-Kuan, NING Ruo-La. Phys. Med. Biol., 2004, **49**(10): 1865–1880